


2016-06-01

## Modification of the In Vitro Uptake Mechanism and Anti-Oxidant Levels in HaCaT Cells and Resultant Changes to Toxicity and Oxidative Stress of G4 and G6 Poly (amido amine) Dendrimer Nanoparticles.

Marcus Maher  
*Technological University Dublin*

Hugh J. Byrne  
*Technological University Dublin, hugh.byrne@tudublin.ie*

Follow this and additional works at: <https://arrow.tudublin.ie/nanolart>

 Part of the [Other Biochemistry, Biophysics, and Structural Biology Commons](#), and the [Toxicology Commons](#)

### Recommended Citation

Maher, M. and Byrne, H., (2016) Modification of the in vitro uptake mechanism and anti-oxidant levels in HaCaT cells and resultant changes to toxicity and oxidative stress of G4 and G6 Poly (amido amine) dendrimer nanoparticles. *Analytical and Bioanalytical Chemistry*, 408, 5295-5307 (2016)

This Article is brought to you for free and open access by the NanoLab at ARROW@TU Dublin. It has been accepted for inclusion in Articles by an authorized administrator of ARROW@TU Dublin. For more information, please contact [yvonne.desmond@tudublin.ie](mailto:yvonne.desmond@tudublin.ie), [arrow.admin@tudublin.ie](mailto:arrow.admin@tudublin.ie), [brian.widdis@tudublin.ie](mailto:brian.widdis@tudublin.ie).



This work is licensed under a [Creative Commons Attribution-Noncommercial-Share Alike 3.0 License](#)

1 Modification of the *in vitro* uptake mechanism and anti-oxidant levels in  
2 HaCaT cells and resultant changes to toxicity and oxidative stress of G4  
3 and G6 Poly (amido amine) dendrimer nanoparticles.

4  
5 Marcus A. Maher<sup>1,2,\*</sup>, Hugh J. Byrne<sup>1</sup>

6  
7 <sup>1</sup>FOCAS Research Institute, Dublin Institute of Technology, Kevin Street, Dublin 8, Ireland

8 <sup>2</sup>School of Physics, Dublin Institute of Technology, Kevin Street, Dublin 8, Ireland

9  
10 \*Corresponding author: marcus.maher@mydit.ie

11  
12  
13 **Keywords:**

14 Dendrimer nanoparticles

15 PAMAM nanoparticles

16 Endocytosis

17 Passive diffusion

18 Oxidative stress

19 Membrane permeability

20 Abstract:

21 The mechanism of cellular uptake by endocytosis and subsequent oxidative stress has been  
22 identified as the paradigm for the toxic response of cationically surface charged nanoparticles. In  
23 an attempt to circumvent the process, the effect of increased cellular membrane permeability on  
24 the uptake mechanisms of poly (amidoamine) dendrimers generation 4 (G4) and 6 (G6) *in vitro*  
25 was investigated. Immortalised, non-cancerous human keratinocyte (HaCaT) cells were treated  
26 with DL-Buthionine-(S,R)-sulfoximine (BSO). Active uptake of the particles was monitored  
27 using fluorescence microscopy to identify and quantify endosomal activity and resultant  
28 oxidative stress, manifest as increased levels of reactive oxygen species, monitored using the  
29 carboxy-H<sub>2</sub>DCFDA dye. Dose dependent cytotoxicity for G4 and G6 exposure was registered  
30 using the cytotoxicity assays Alamar Blue and MTT, from 6 to 72 hours.

31 Reduced uptake by endocytosis is observed for both dendrimer species. A dramatic change,  
32 compared to untreated cells, is observed in the cytotoxic and oxidative stress response of the  
33 BSO treated cells. The significantly increased mitochondrial activity, dose dependent anti-  
34 oxidant behaviour and reduced degree of endocytosis for both dendrimer generations, in BSO  
35 treated cells, indicates enhanced permeability of the cell membrane, resulting in the passive,  
36 diffusive uptake of dendrimers, replacing endocytosis as the primary uptake mechanism. The  
37 complex MTT response reflects the importance of glutathione in maintaining redox balance  
38 within the mitochondria. The study highlights the importance of regulation of this redox balance  
39 for cell metabolism, but also points to the potential of controlling the nanoparticle uptake  
40 mechanisms, and resultant cytotoxicity, with implications for nanomedicine.

41

## 42 Introduction

43 Nanoparticle science is a rapidly advancing field which holds much promise in areas such as  
44 targeted drug and gene delivery.<sup>1,2,3</sup> However, nanoparticle uptake into a cell has been  
45 demonstrated, particularly for nanoparticles with an effective cationic surface charge, to give rise  
46 to cytotoxic responses, raising concerns about the potential health and environmental impact of  
47 the proliferation of nanomaterials in consumer products.<sup>4</sup> A systematic understanding of the  
48 mechanisms of toxicity and their dependence on nanoparticle physico-chemical properties on a  
49 cellular level is therefore required.<sup>5</sup> In the context of nanomedical applications, understanding  
50 and controlling the uptake process and subcellular trafficking of the delivery vehicle and the  
51 bioavailability of the cargo are critically important.

52  
53 Cellular uptake of nanoparticles principally occurs via endocytosis, whereby the nanoparticle is  
54 invaginated by the cellular membrane and is transported into the cell.<sup>6</sup> As the low pH  
55 environment of the endosome attempts to digest the nanoparticle, the redox balance of the cell is  
56 disrupted, and, in the case of nanoparticles with an effective cationic surface charge, the process  
57 gives rise to an increase in the production of Reactive Oxygen Species (ROS), localised mainly  
58 around the endosome (or later lysosome).<sup>6,7,8,9</sup> Although intra cellular anti-oxidants attempt to  
59 neutralise the imbalance, ROS production can be sufficient to lead to oxidative stress.<sup>10</sup>  
60 Subsequently, a cascade of events and the release of several characteristic cytokines and  
61 chemokines occurs, ultimately leading to cell death, a process which is the accepted paradigm of  
62 nanotoxicity of many nanoparticles *in vitro*.<sup>6</sup> The process has been well demonstrated for model  
63 nanoparticle system such as amine functionalised polystyrene,<sup>11,12,13</sup> amorphous nanosilica,<sup>14</sup> and  
64 nanomeric polymeric dendrimers.<sup>10</sup>

65  
66 Aminated molecules are intrinsic antioxidants, however, and generally regarded as ROS  
67 scavengers. As examples, spermine and spermidine have both been shown to reduce  $\text{Fe}^{3+}$  to  $\text{Fe}^{2+}$   
68 <sup>15</sup> and the ferric reducing activity of these molecules has been identified as a measure of anti-  
69 oxidant potential.<sup>16</sup> Carnosine, an endogenous dipeptide, has been shown to scavenge both  
70 reactive oxygen and nitrogen species.<sup>17</sup> Notably, in a study by Khalid *et al.* (2015), while the  
71 larger, higher generations of the aminated nanoscale dendrimers Poly (propylene imine) (PPI)  
72 were demonstrated to elicit oxidative stress and significant toxicity, the smaller, lower  
73 generations exhibited intracellular antioxidant behaviour and low toxicity.<sup>18</sup> Examination of the  
74 uptake mechanisms indicated a transition from cellular uptake by passive diffusion at low  
75 generations to active endocytosis for higher generations. The study suggests that, in the case of  
76 catatonically charge nanoparticles, the endocytotic uptake and trafficking process is, in itself, a  
77 source of cellular toxicity. In the context of drug delivery, invagination of the delivery vehicle  
78 and cargo in this harsh environment may also be undesirable, and although escape by  
79 endosomolysis is a potential strategy,<sup>19</sup> this too can be a harsh process, causing significant  
80 damage to the cell.<sup>20,21</sup> For these reasons, circumventing endocytosis appears to be a valid  
81 strategy for the reduction of toxicity associated with aminated nanoparticles as well as  
82 nanoparticle drug or gene delivery.  
83  
84 Guarnieri *et al.* (2015), demonstrated that functionalization of aminated polystyrene  
85 nanoparticles with the viral peptide gH625 (derived from *Herpes simplex virus – 1*), which has a  
86 membrane perturbing domain, enables translocation of particles to the cytoplasm, avoiding  
87 endocytosis and thus, dramatically reducing the cytotoxicity.<sup>22</sup> An alternative strategy to increase

88 the permeability of the cellular membrane, *in vitro*, is through the application of DL-Buthionine-  
89 (*S,R*)-sulfoximine (BSO). BSO has previously been employed to study the effects of the  
90 reduction of levels of the intracellular antioxidant glutathione (GSH); and therefore oxidative  
91 stress<sup>23,24,25,26</sup> and has been shown to cause membrane permeabilisation.<sup>27,28</sup> BSO works as an  
92 inhibitor of the enzyme Glutamate Cysteine Ligase (EC 6.3.2.2) (historically known as gamma-  
93 glutamylcysteine synthetase) which is the first step in the production of GSH in the cell.<sup>29</sup> This  
94 reduction in GSH causes several different effects, one being the induction of the membrane  
95 permeability transition in the mitochondria.<sup>30,31,32</sup> The opening of this pore and the depletion of  
96 GSH allows ROS to diffuse from the mitochondria to the cell and via lipid peroxidation, cause  
97 damage to the cell membrane,<sup>28</sup> leading to increased permeability.

98  
99 The reduction of GSH in the cell can have other adverse effects, however, mainly due to the fact  
100 that GSH is one of the main antioxidants involved in maintaining the redox balance of the  
101 mitochondria.<sup>33</sup> In the mitochondria, endogenous ROS is produced as a by-product of normal  
102 metabolism and therefore completely eliminating GSH can leave the cell susceptible to damage  
103 from this ROS.<sup>34</sup> Furthermore, reductions in cellular GSH can also lead to changes in the  
104 regulation of Ca<sup>2+</sup> distribution<sup>35,36,37</sup> and the activation/deactivation of signalling pathways  
105 involved with growth, differentiation and apoptosis.<sup>33,38,39,40</sup> The loss of GSH and subsequent  
106 changes in the cell have been implicated in several disease states which is reviewed elsewhere.<sup>34</sup>

107  
108 This study explores the impact, for HaCaT cell, of BSO treatment on the cellular uptake of, and  
109 subsequent oxidative stress and toxic response to, poly (amido amine) (PAMAM) dendrimers.  
110 These nanoscale aminated dendrimers have a systematically variable molecular structure, and the

111 homologous series of increasing generation, and concomitant size and number of surface amino  
112 groups, has been demonstrated to be ideal to study the dependence of nanoparticle cellular  
113 interactions on the physico-chemical properties of the particles. Previous studies have examined  
114 the structurally dependent toxicity, and underlying mechanisms of endocytosis, oxidative stress,  
115 immune responses and consequent toxicity<sup>7,8,9,10</sup> and the responses have been numerically  
116 modelled, as a guide towards a predictive toxicology approach.<sup>10,41</sup> For consistency and to allow  
117 comparisons with the previous work, the *in vitro* studies reported here were also carried out  
118 using the immortalised human keratinocyte cell line, HaCaT, and identical oxidative stress and  
119 cytotoxic assays. Furthermore, PAMAM dendrimers of Generation 4 and 6 were chosen as the  
120 extremes of the previously reported cytotoxicological response. In comparison, it is  
121 demonstrated that treatment with BSO results in a significant change in the nanoparticle uptake  
122 mechanisms and cytotoxicity.

123 Materials and Methods

124 Materials

125 DMEM F12 HAM growth medium, Penicillin, Streptomycin, fluorescently labelled, Polystyrene  
126 nanoparticles, with amine surface modification (PSNP-NH<sub>2</sub>) 100nm, DL-Buthionine-(*S,R*)-  
127 sulfoximine(BSO) and 3-(4,5-dimethylthiazol-2-yl)-2,5-diphenyltetrazolium bromide (MTT) dye  
128 were purchased from Sigma-Aldrich, Ireland. The PAMAM dendrimer nanoparticles,  
129 generations 4 (molecular weight: 14,214 g/mol) and 6 (molecular weight: 58,046 g/mol), were  
130 purchased from Sigma-Aldrich and manufactured by Dendritech Inc. ThiolTracker™ Violet  
131 (TTV), CellLight® Early Endosomes-RFP, BacMam 2.0, Fetal Bovine Serum (FBS), L-  
132 Glutamine, Alamar Blue (AB) and 5-(and-6)-carboxy-2',7'-dichlorodihydrofluorescein diacetate  
133 (carboxy-H<sub>2</sub>DCFDA) dye were purchased from Life Technologies™, Bio-Sciences, Ireland.  
134 HaCaT cells were purchased from Cell Line Services (CLS), Eppelheim, Germany. TrueLine 96-  
135 well cell culture plates were used for all viability and ROS studies.

136 All fluorescence and absorbance readings were taken on a Molecular Devices SpectraMax M3  
137 Spectrometer. Confocal Laser Scanning Fluorescence Microscopy (CLSM) images were taken  
138 on a Zeiss LSM 510 Confocal Laser Scanning Microscope and processed using ImageJ software  
139 (with co-localisation analysis performed with the JaCoP plugin for ImageJ). All viability, ROS  
140 and GSH data analysis was performed using SigmaPlot v10.0 software.

141

142 Methods

143 Cell culture

144 HaCaT cells are an immortalised, non cancerous human keratinocyte cell line and were used for



145 these experiments. The cells were cultured in DMEM F12 HAM supplemented with 10% FBS,  
146 45 IU/mL penicillin, 45 IU/mL streptomycin and 2mM L-glutamine at 37°C in 5% CO<sub>2</sub>.  
147 All assays carried out in this set of experiments were performed in 96 well plates, with cells  
148 plated at a concentration of 1x10<sup>4</sup> cells/well in 100µL of DMEM medium. Cells were allowed 24  
149 hours to attach and were then treated with BSO for an additional 18 hours (at a concentration of  
150 200µM), after which cells were exposed to PAMAM G4 or G6 dendrimers (in DMEM F12  
151 HAM, with 5%FBS, 45 IU/mL penicillin, 45 IU/mL streptomycin, 2mM L-glutamine and  
152 200µM BSO) at various concentrations for the specified time points. Six replicates of each  
153 concentration were performed per plate and each plate was repeated in triplicate.

154

#### 155 ThiolTracker™ Violet (TTV)

156 ThiolTracker™ Violet (TTV) is a GSH detection agent. Cells were plated as described above and  
157 a concentration gradient of BSO was applied. Cells were left for 18 hours at 37°C in 5% CO<sub>2</sub> to  
158 allow for reduction of the amount of intracellular GSH. Cells were then washed twice with PBS,  
159 100µL of TTV dye (at a final concentration of 20µM) were added to each well and the plates  
160 were allowed to incubate at 37°C in 5% CO<sub>2</sub> for 30 minutes, after which the TTV solution was  
161 removed and replaced with PBS. The fluorescence of each well was then read using the  
162 SpectraMax M3 spectrometer with  $\lambda_{EX}$ = 404nm and  $\lambda_{EM}$ = 526nm. GSH values were calculated  
163 as compared to the unexposed control.

164

#### 165 Viability assays

166 Alamar Blue and MTT assays were used to determine the changes in cell viability, after  
167 treatment with BSO as described above, as a result of exposure to both PAMAM G4 and G6

168 dendrimers. Both Alamar Blue and MTT were performed on the same plate. The PAMAM G4  
169 concentrations used were: 0.16, 0.32, 0.65, 1.3, 2.6, 5.2, 7.8 and 10.4 $\mu$ M, while the PAMAM G6  
170 concentrations were: 0.08, 0.16, 0.32, 0.65, 1.3, 2.6, 3.9 and 5.2 $\mu$ M. The lower initial value of  
171 the PAMAM G6 dendrimers was used due to their reported EC<sub>50</sub> value being much lower than  
172 their G4 counterparts.<sup>7,8,9</sup> Dose dependent viability percentages were calculated at time points: 6,  
173 12, 24, 48 and 72 hours. Percentage viability was calculated as compared to a control which had  
174 been exposed to 200 $\mu$ M BSO, but had no nanoparticle treatment; this was to ensure any changes  
175 were caused by the nanoparticle and were not the result of BSO treatment. A separate control  
176 where no BSO was present was also performed and showed there was little difference between  
177 cells with no BSO exposure and cells which were exposed to BSO (Supplementary Material,  
178 Figure: S1).

179

#### 180 Alamar Blue (AB)

181 The Alamar Blue assay was made up from 10X stock solution in medium (DMEM F12 HAM,  
182 with no additional supplements). At the specified time point, the plates were removed from the  
183 incubator and the medium containing PAMAM dendrimer was removed, the cells were washed  
184 with 100 $\mu$ L PBS and then 100 $\mu$ L of DMEM F12 HAM(unsupplemented) containing Alamar  
185 Blue were added to each well. The plates were incubated for 3 hours at 37°C in 5% CO<sub>2</sub> to allow  
186 for conversion of the dye. The fluorescence of each well was then read using the SpectraMax M3  
187 spectrometer with  $\lambda_{EX}$ = 555nm and  $\lambda_{EM}$ = 585nm.

188

#### 189 MTT (3-(4,5-dimethylthiazol-2-yl)-2,5-diphenyltetrazolium bromide)

190 A stock solution of MTT was made at a concentration of 0.5mg/mL. 500 $\mu$ L of this stock were  
191 added for every 10mL of medium (DMEM F12 HAM, with no additional supplements). At the  
192 specified time point, the plates were removed from the incubator and the medium containing  
193 PAMAM dendrimer was discarded, the cells were washed with 100 $\mu$ L PBS and then 100 $\mu$ L of  
194 DMEM (unsupplemented) containing MTT was added to each well. The plates were incubated  
195 for 3 hours at 37°C in 5% CO<sub>2</sub> to allow for conversion of the dye. After 3 hours, any remaining  
196 dye was removed and each well was again washed with 100 $\mu$ L PBS, after which 100 $\mu$ L of  
197 DMSO was added and the plates were placed on a shaker for 10 minutes to allow for the dye to  
198 solubilise. The absorbance of each well was then read using the SpectraMax M3 spectrometer  
199 with  $\lambda_{\text{ABS}}=595\text{nm}$ .

200

#### 201 Reactive Oxygen Species (ROS)

202 5-(and-6)-carboxy-2',7'-dichlorodihydrofluorescein diacetate (carboxy-H<sub>2</sub>DCFDA) dye was used  
203 for the detection of ROS. The dye was made up to a final concentration of 10 $\mu$ M in sterile PBS.  
204 Before addition of PAMAM dendrimer, this dye was added to the cells and allowed to incubate  
205 for 1 hour, after which, the dye was removed, the cells were washed thrice with PBS and the  
206 medium containing PAMAM dendrimer was added. At the specified time points the fluorescence  
207 was read by the SpectraMax M3 spectrometer with  $\lambda_{\text{EX}}=488\text{nm}$  and  $\lambda_{\text{EM}}=535\text{nm}$ .

208

#### 209 Confocal Laser Scanning Microscopy (CLSM)

210 Cells were plated onto MatTek 35mm glass bottom dishes at a concentration of 20,000 cells/dish  
211 in DMEM F12 HAM (supplemented with 10% FBS, 45 IU/mL penicillin, 45 IU/mL  
212 streptomycin and 2mM L-glutamine) and allowed to attach for 4 hours, at which point the

213 medium was removed and replaced with medium containing Celllight<sup>®</sup> Early Endosomes-RFP,  
214 BacMam 2.0 at a concentration of 20 particles per cell. Early endosome formation was tracked  
215 with the Celllight<sup>®</sup> Early Endosome – RFP kit, which transfects, into the cell, a version of Rab5a  
216 with a bound Red Fluorescent Protein. The cells were allowed to incubate (37°C, 5% CO<sub>2</sub>) for 16  
217 hours to ensure transfection with the early endosome reagent. After this, the medium was  
218 removed and cells were washed twice with PBS. For cells being tested without BSO, medium  
219 was added for 18 hours (these samples are referred to as untreated cells/untreated controls in the  
220 text), while for cells being tested with BSO, medium containing 200µM BSO was added for 18  
221 hours. Cells were again washed with PBS and carboxy-H<sub>2</sub>DCFDA was added for 1 hour (10µM  
222 in 2mL PBS), after which cells were again washed twice with PBS. PAMAM dendrimers were  
223 added at a concentration of 3.21µM (G4) and 1µM (G6) and cells were allowed to incubate for 3  
224 hours (G4) or 1 hour (G6) and were then washed twice with PBS and imaged with the Zeiss  
225 LSM 510 Confocal Laser Scanning Microscope. 100nm PSNP-NH<sub>2</sub> with attached Green  
226 Florescent Protein was used as a positive control to ensure the Celllight<sup>®</sup> Early Endosomes-RFP  
227 was functioning as expected; the results of this test are available in the supplementary material  
228 section, Figure S2. Negative controls were also performed with cells which were not exposed to  
229 any nanoparticles, and little to no fluorescence was noted (data not shown). For ROS monitoring,  
230 doses and time points noted above were chosen based on the maximum responses previously  
231 reported in literature.<sup>8</sup> All confocal images were analysed using ImageJ and co-localisation  
232 studies were performed using Manders split coefficients calculated with the JaCoP plugin for  
233 ImageJ.<sup>42</sup>

234

235 Data Analysis and Statistics

236 Data analysis was performed using SigmaPlot™ v10.0 and fluorescence was calculated based on  
237 the values of BSO controls (which were unexposed to nanoparticles, but had been treated with  
238 200µM BSO for 18 hours).

239 “The cytotoxicity, GSH and ROS experiments were performed in 96-well microplates with six  
240 replicates per plate and each plate repeated three times. Therefore, data points shown represent  
241 the mean of 18 points, with error bars representing  $\pm$  the standard deviation (as calculated by  
242 SigmaPlot™ v10.0). Confocal Images were taken on a Zeiss LSM 510 and processed using  
243 ImageJ software. Images were taken of eight cells/groups of cells and the images presented in the  
244 manuscript are representative of the sampled cell population.”

245

## 246 Results

### 247 BSO treatment

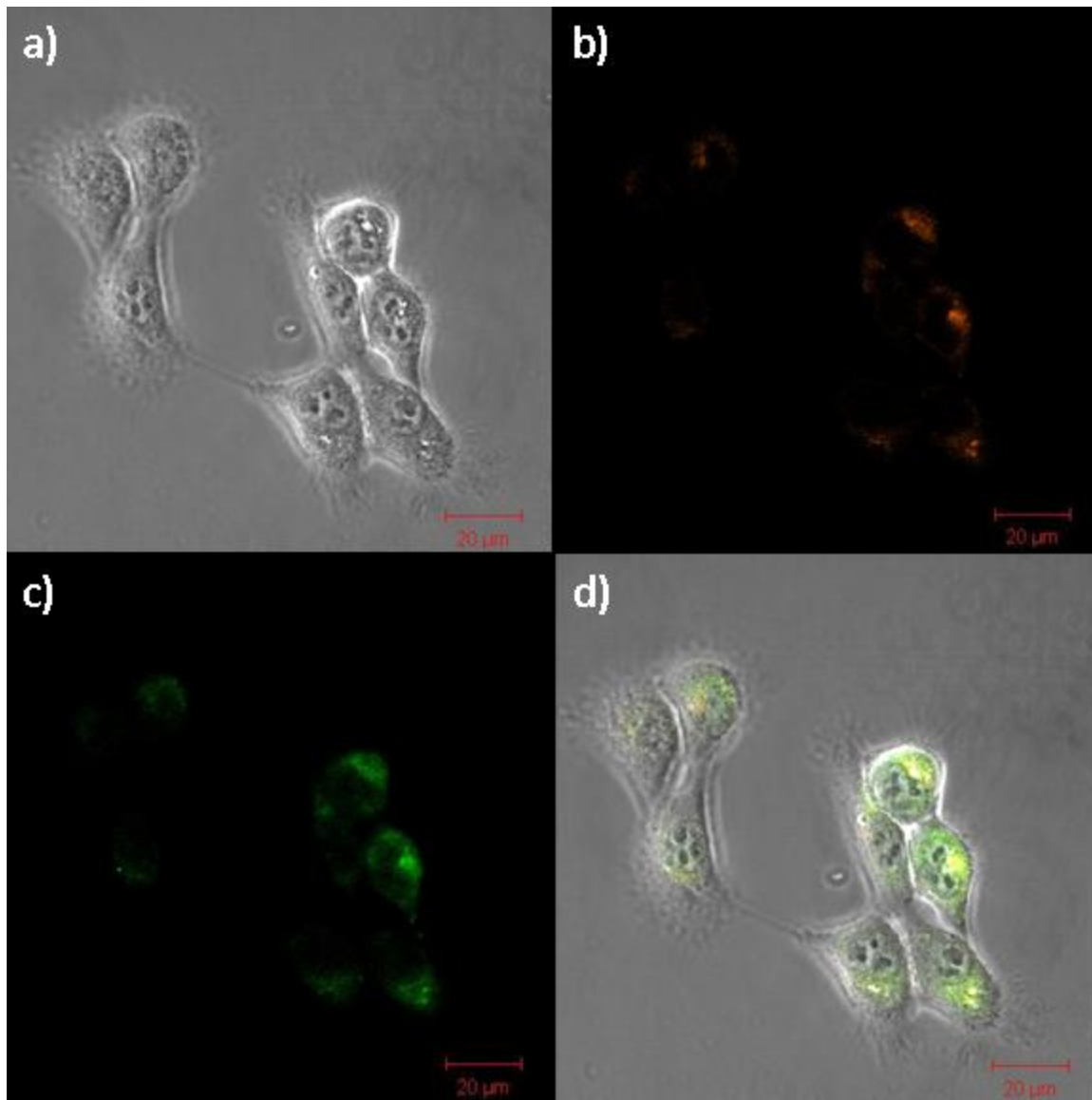
248 While maximising the desired effect of the BSO on the cells, it is important that the viability of  
249 the cells is not affected. TTV showed a 40% reduction in intracellular levels of GSH for the  
250 HaCaT cells upon 200µM BSO exposure for 18 hours (adapted from the methods of: He *et al.*  
251 (2003)).<sup>24</sup> This dose and time point were found to have a minimal impact on cellular viability as  
252 measured by the AB and MTT assays (data available in Supplementary Material, Figure: S3).  
253 Higher concentrations were found to have an effect on cellular viability, although a more  
254 pronounced effect was observed by CLSM, where signs of cellular stress were noted (data not  
255 shown). Therefore 200µM BSO exposure was chosen as optimal.

256

### 257 PAMAM G4 dendrimers

258 CLSM was employed as a way to examine the effect of BSO treatment on the cellular uptake  
259 mechanisms and subsequent oxidative stress. Early endosome formation was tracked with the  
260 Celllight<sup>®</sup> Early Endosome – RFP kit and the formation of ROS was also tracked using the  
261 carboxy-H<sub>2</sub>DCFDA dye. Fluorescently labelled PSNP-NH<sub>2</sub> of 100nm diameter were employed  
262 as positive controls, and the results for those are shown in the Supplementary Material: Figure  
263 S2.

264

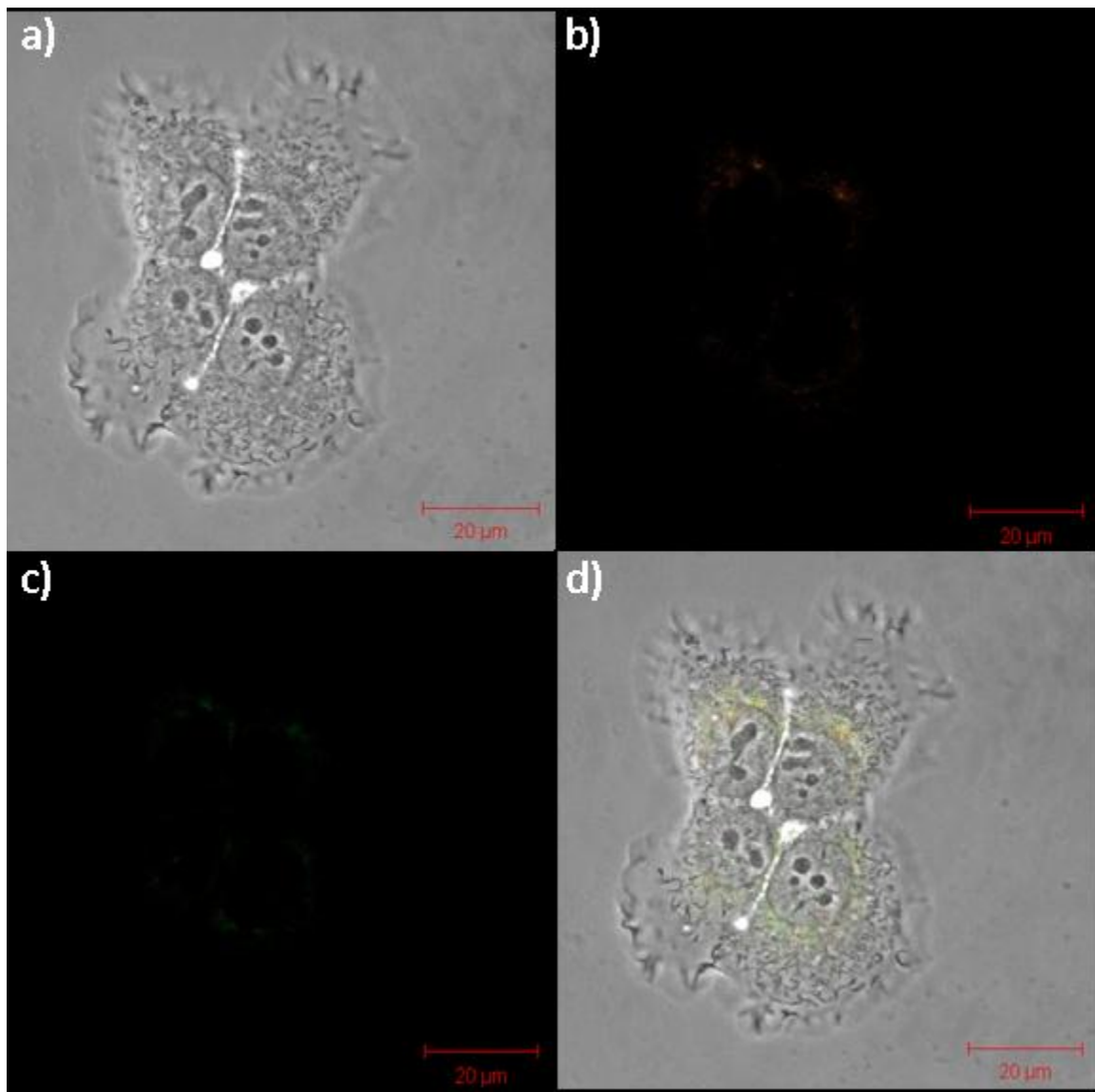


265

266 Figure 1: CLSM images of HaCaT (live) cells, upon exposure to 3.21 μM PAMAM G4  
267 dendrimer at 3 hours (no BSO is present in this sample). Image a) shows the bright field image  
268 of the cells, Image b) shows the fluorescence generated by the early endosomal red fluorescent  
269 protein, Image c) shows the fluorescence generated by the ROS (interacting with the carboxy-  
270 H<sub>2</sub>DCFDA dye) and Image d) shows the overlay of images a-c, where yellow coloured areas  
271 indicate simultaneous endosomal and ROS activity.

272

273 Figure 1 shows the HaCaT cells following the reported paradigm of PAMAM G4 endocytosis  
274 and subsequent ROS generation at the endosomal sites.<sup>6,7,8,9</sup> Co-localisation (performed on the  
275 images in Figure 1) shows that 91( $\pm$ 3)% of the generated ROS occurs in the neighbourhood of  
276 endosomes, and that 71( $\pm$ 4)% of endosomal formation resulted in increases in ROS production  
277 (the other 30% of endosomal activity is most likely due to endocytosis which would be routinely  
278 done by the cell and would not involve the dendrimers and therefore not produce ROS).  
279



280



281 Figure 2: Confocal images of HaCaT (live) cells, upon exposure to 3.21 $\mu$ M PAMAM G4  
282 dendrimer at 3 hours, with pre-treatment of BSO: 200 $\mu$ M for 18hours. Image a) shows the bright  
283 field image of the cells, Image b) shows the fluorescence generated by the early endosomal red  
284 fluorescent protein, Image c) shows the fluorescence generated by the ROS (interacting with the  
285 carboxy-H<sub>2</sub>DCFDA dye) and Image d) shows the overlay of images a-c, where yellow coloured  
286 areas indicate simultaneous endosomal and ROS activity.

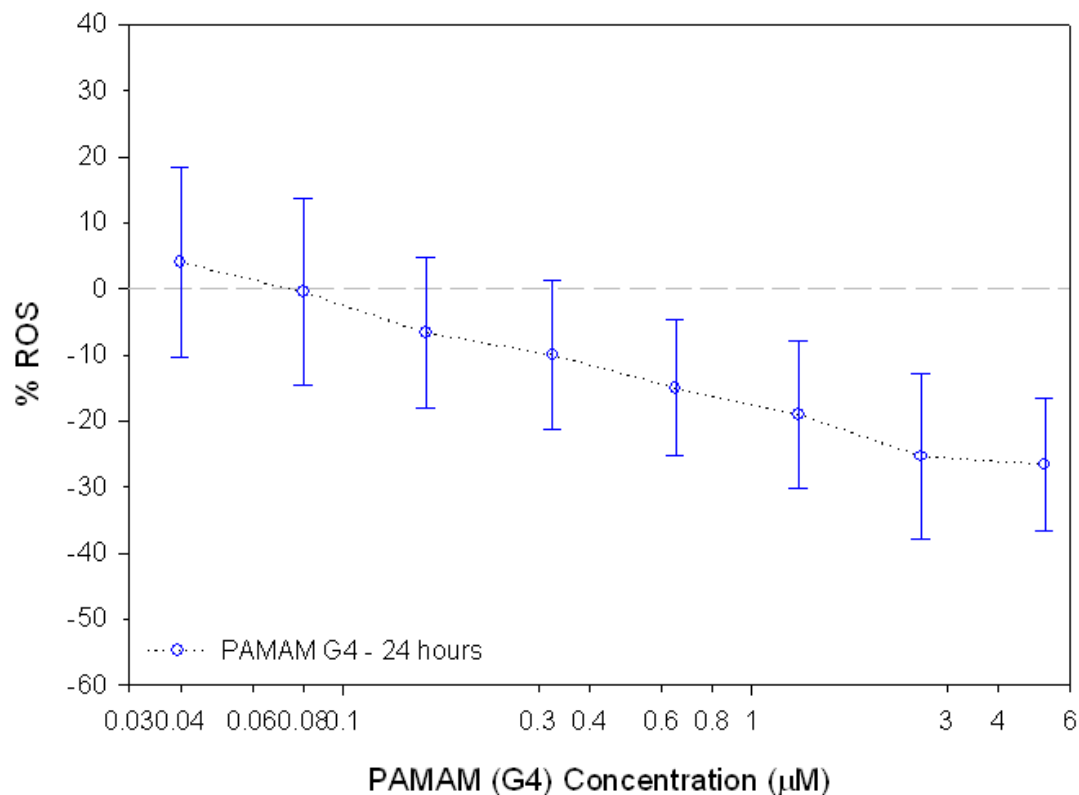
287

288 In contrast, Figure 2 shows HaCaT cells which have been treated with BSO for 18 hours prior to  
289 PAMAM G4 exposure (BSO was still present in the media upon exposure, to ensure conditions  
290 were consistent). In images (b) and (c), the intensity of the endosomal RFP and ROS dye have  
291 been significantly reduced. Again co-localisation analysis was performed (on images in Figure 2)  
292 and showed that 30( $\pm$ 6)% of the generated ROS was happening around the endosomes, and that  
293 46( $\pm$ 14)% of endosomal formation resulted in increases in ROS production. Intensity analysis of  
294 the red fluorescent protein produced by endocytosis, on average, showed a reduction in intensity  
295 of 70( $\pm$ 3)% for cells treated with BSO.

296

297 Endosomal uptake was clearly reduced, although a decrease in the intensity of response of the  
298 ROS detection dye, carboxy-H<sub>2</sub>DCFDA, was also noted, prompting a quantitative analysis of the  
299 ROS contents of the HaCaT cells: Figure 3.

300



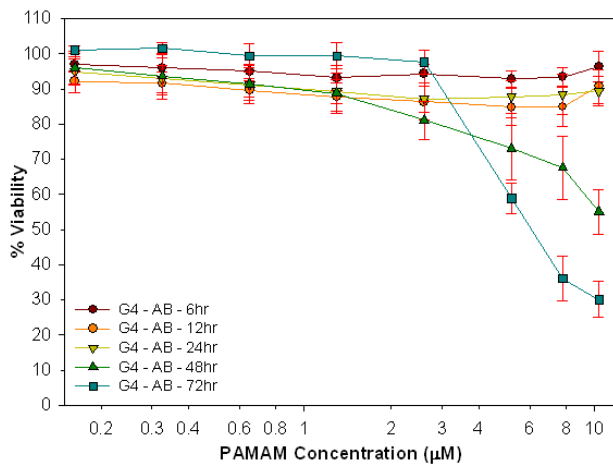
301  
 302 Figure 3: Dose dependant generation of ROS in HaCaT cells (shown for 24 hours for the  
 303 PAMAM G4). ROS is compared to BSO control which was set to equal 0%. The X-axis is  
 304 plotted logarithmically to allow for better visualisation of lower concentrations. Data points are  
 305 the mean of 18 samples, with error bars showing ( $\pm$ ) the standard deviation.  
 306  
 307 The analysis of ROS showed a net decrease at all doses tested; for clarity, only the dose  
 308 dependence of the 24 hour test has been shown, the full data-set is available in the supplementary  
 309 material section (Figure S4). Over the dose range tested, the ROS response followed a  
 310 monotonically decreasing trend. This result, is again, in contrast with previous observations, in  
 311 which ROS levels were seen to increase above control levels in a dose dependant fashion, upon  
 312 G4 dendrimer exposure.<sup>8</sup>

313

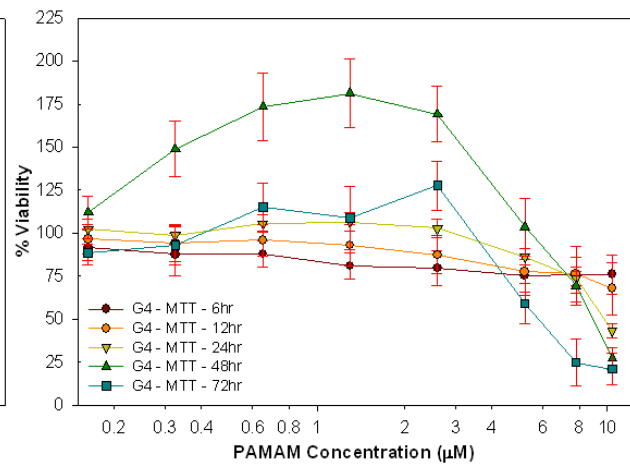
314 To examine how these changes in both endocytosis and ROS production affected the viability of  
 315 the cell AB and MTT assays were performed. HaCaT cells were exposed to 200 $\mu$ M BSO for 18  
 316 hours and subsequently exposed to varying concentrations of PAMAM G4 nanoparticles.  
 317 Viability was measured at 6, 12, 24, 48 and 72 hours (Figure 4 (a) and (b)).

318

319 (a)



(b)



320

321 Figure 4: Alamar Blue (a) and MTT (b) dose dependant viability results for PAMAM G4

322 dendrimers in HaCaT cells after 6, 12, 24, 48 and 72 hours. Viability is calculated as the

323 percentage of living cells as compared to BSO control. Data points are the mean of 18 samples,

324 with error bars showing ( $\pm$ ) the standard deviation.

325

326 The AB assay shows little or no toxicity of PAMAM G4 at time points 6, 12, and 24 hours,

327 whereas the viability is reduced to 50% at 48 hours and 30% at 72 hours, for the higher dose

328 exposures. In HaCaT cells which have not been treated with BSO, the  $EC_{50}$  obtained from AB is

329 around 10 $\mu$ M at 24 hours,<sup>7</sup> whereas, in Figure 4, at the same time point, it is clear that there is no

330 significant toxicity. The MTT results show a dramatically different dose dependent cytotoxicity

331 profile for the BSO dosed cells compared to un-dosed.<sup>7</sup> At 6 hours exposure (Figure 4b), the

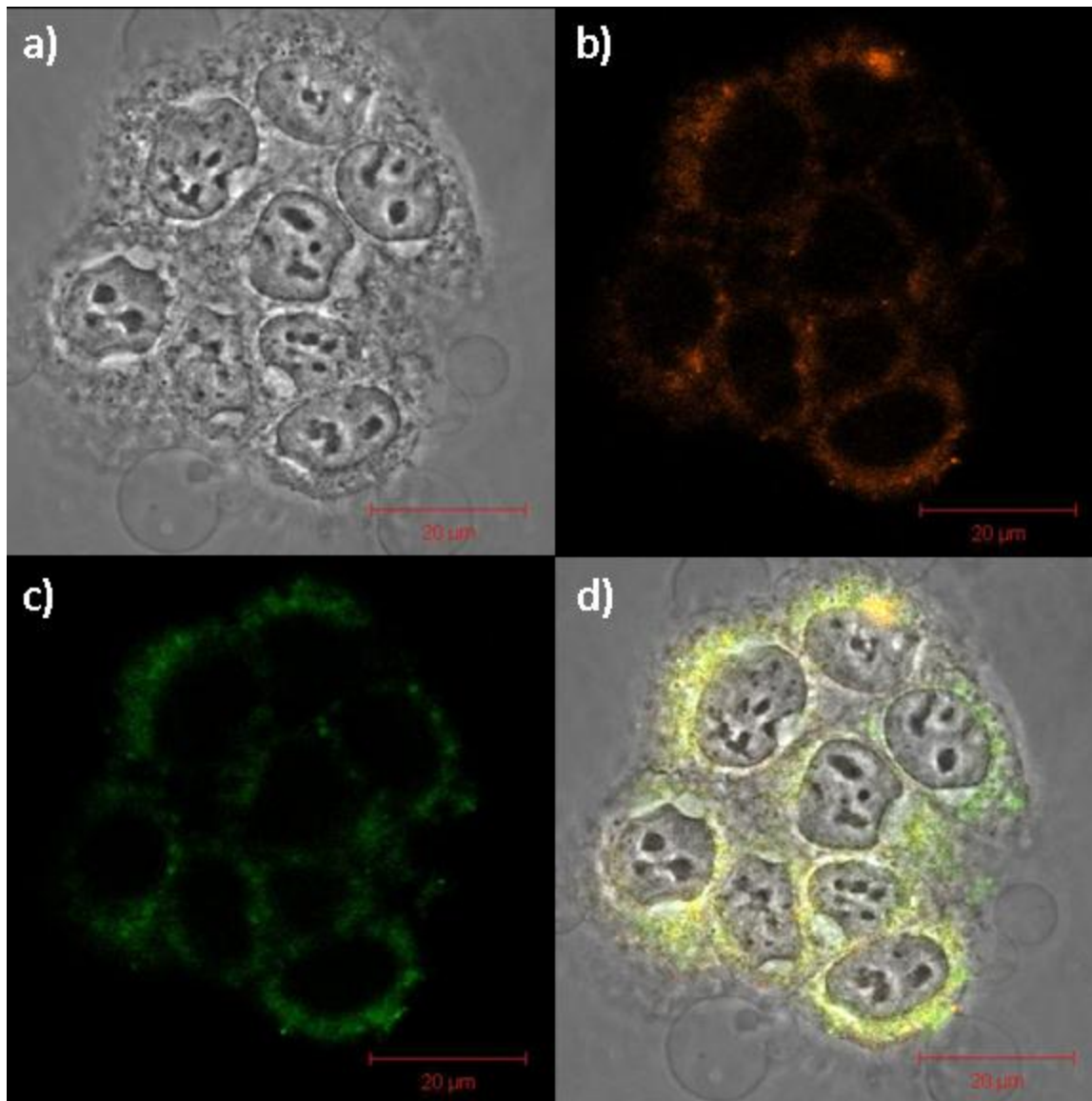
332 viability is seen to be reduced to around 80% over the entire dose range. However, at exposure  
333 times of 12, 24, 48 and 72 hours, increases in viability are seen for the low-medium dose range.  
334 The effect is particularly pronounced at the 48 hour time point, at which the recorded MTT  
335 response is ~175% of control, for an exposure dose of ~1 $\mu$ M. For doses of ~2.6 $\mu$ M and higher,  
336 the MTT assay response registers a decrease in viability, which is more pronounced in the longer  
337 time point exposures.

338

### 339 PAMAM G6 dendrimers

340 Analysis of uptake and ROS production was again carried out using CLSM (with the same  
341 method as the PAMAM G4) incorporating the carboxy-H<sub>2</sub>DCFDA dye and Celllight<sup>®</sup> Early  
342 Endosome – RFP kit (Figure 5 and 6).

343



344

345 Figure 5: Confocal images of HaCaT (live) cells, upon exposure to 1μM PAMAM G6 dendrimer

346 at 1 hour (no BSO is present in this sample). Image a) shows the bright field image of the cells,

347 Image b) shows the fluorescence generated by the early endosomal red fluorescent protein,

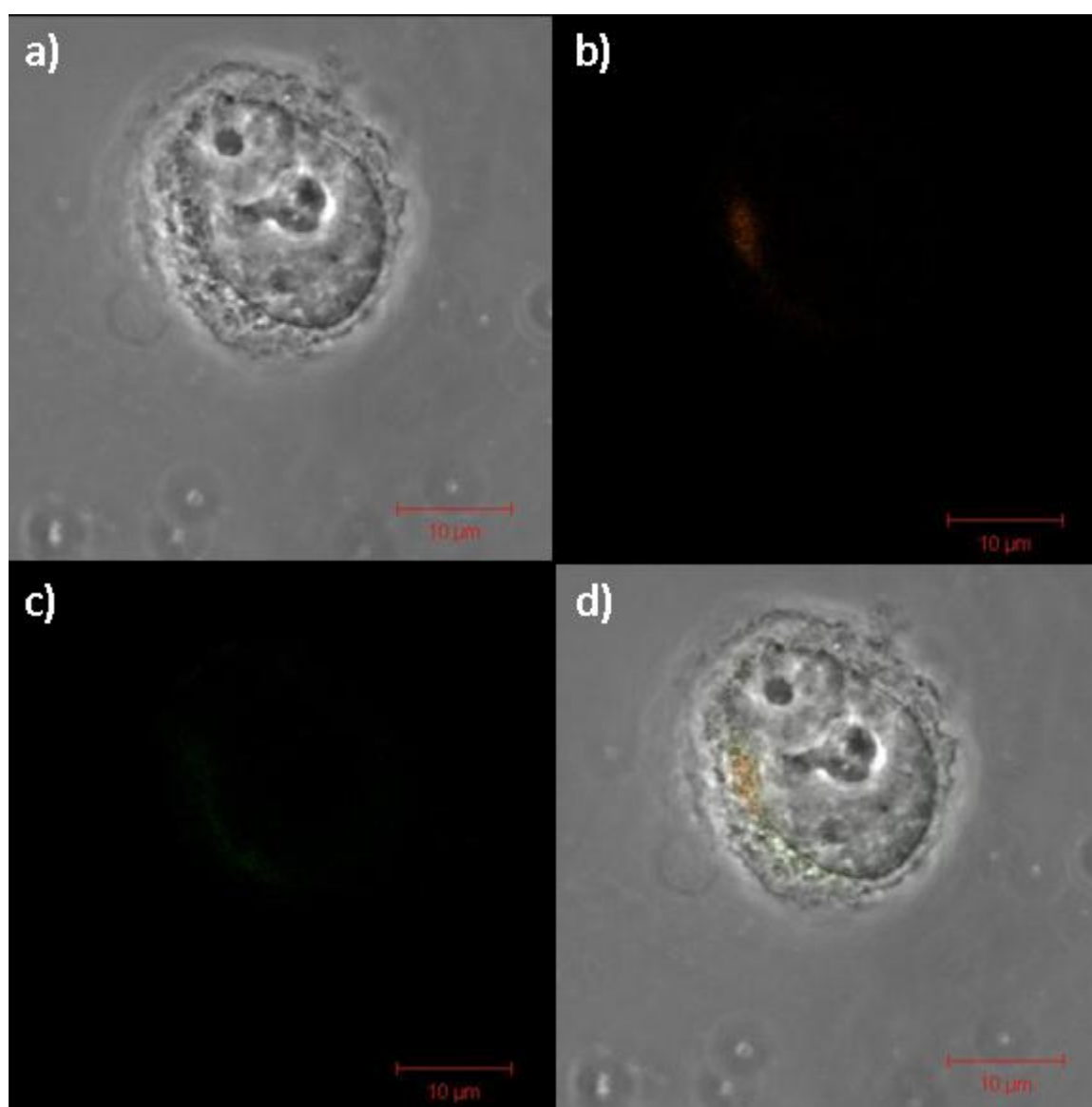
348 Image c) shows the fluorescence generated by the ROS (interacting with the carboxy-H<sub>2</sub>DCFDA

349 dye) and Image d) shows the overlay of images a-c, where yellow coloured areas indicate

350 simultaneous endosomal and ROS activity.

351

352 In the absence of BSO, PAMAM G6 exposure, resulted in strong red fluorescence indicating a  
353 high level of endocytosis, complemented by strong green fluorescence indicating increased ROS  
354 production. Co-localisation analysis (of images in Figure 5) found that  $75(\pm 2)\%$  of the generated  
355 ROS occurred in the region of the endosomes, and that  $92(\pm 1)\%$  of endocytosis resulted in  
356 increases in ROS production. This strong level of co-localisation is indicative of the accepted  
357 paradigm of nanoparticle uptake by endocytosis, and ROS production at the site of endosomes.  
358



359

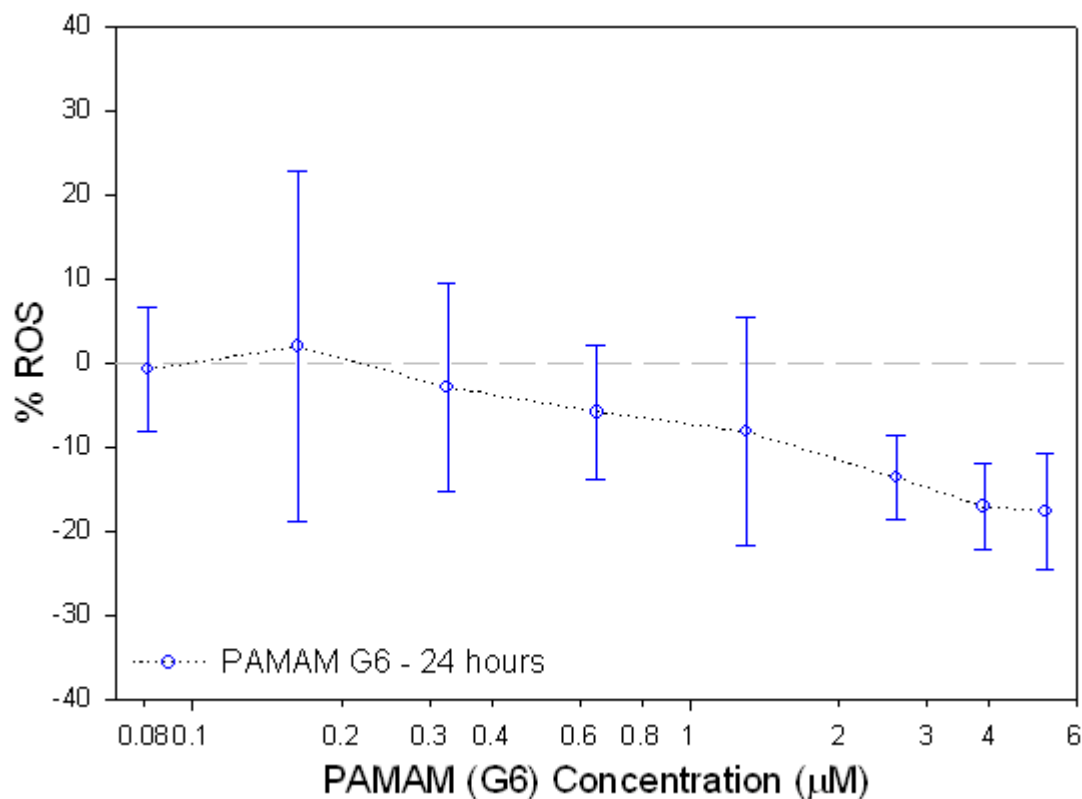
360 Figure 6: Confocal images of HaCaT (live) cells, upon exposure to 1 $\mu$ M PAMAM G6 dendrimer  
361 at 1 hour, with pre-treatment of BSO: 200 $\mu$ M. Image a) shows the bright field image of the cells,  
362 Image b) shows the fluorescence generated by the early endosomal red fluorescent protein,  
363 Image c) shows the fluorescence generated by the ROS (interacting with the carboxy-H<sub>2</sub>DCFDA  
364 dye) and Image d) shows the overlay of images a-c, where yellow coloured areas indicate  
365 simultaneous endosomal and ROS activity.

366

367 In comparison to exposure of PAMAM G6 in cells without BSO treatment (untreated cells),  
368 there is a sparsity of endosomal activity and oxidative stress response in cells which had been  
369 pre-treated with BSO for 18 hours. Analysis (of the images in Figure 6) showed decreased levels  
370 of co-localisation between the ROS and endosomal formation: only 41( $\pm$ 18)% of ROS  
371 production was recorded in areas where endosomes had formed and 55( $\pm$ 10)% of endocytosis  
372 resulted in increases in ROS production. Intensity analysis of the red fluorescent protein  
373 produced by endocytosis, on average, showed a reduction in intensity of 61( $\pm$ 1)% for cells  
374 treated with BSO when compared to the untreated cells.

375

376 Again, in light of the reduced ROS response, quantitative analysis, using carboxy-H<sub>2</sub>DCFDA  
377 was performed: Figure 7.



378  
 379 Figure 7: Dose dependant generation of ROS in HaCaT cells (shown at 24 hours for the  
 380 PAMAM G6). ROS is compared to BSO control which was set to equal 0%. The X-axis is  
 381 plotted logarithmically to allow for better visualisation of lower concentrations. Data points are  
 382 the mean of 18 samples, with error bars showing ( $\pm$ ) the standard deviation.

383  
 384 The dose response of the ROS generation shows similarities with the G4 in the overall  
 385 progression of the response, pointing to a trend where increasing concentration leads to  
 386 decreasing amounts of ROS, contrary to what has been observed in previous studies without  
 387 BSO exposure.<sup>8</sup> As with the G4 analysis, for clarity, only one of the eight concentrations tested  
 388 have been shown, the full data-set is available in the supplementary material section (Figure S5).  
 389 At all doses tested, the ROS response followed the same trend as shown in Figure 7.

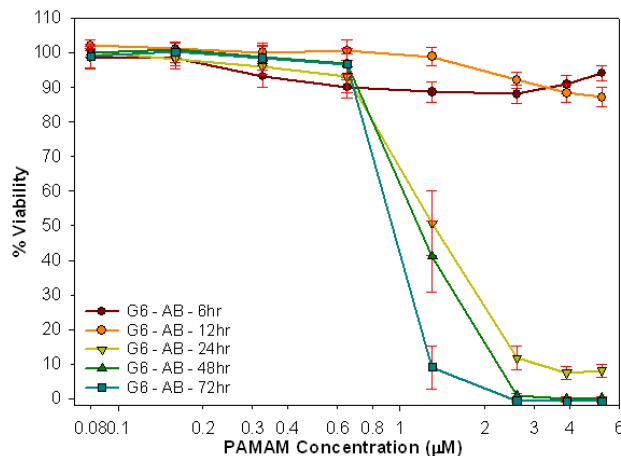
390



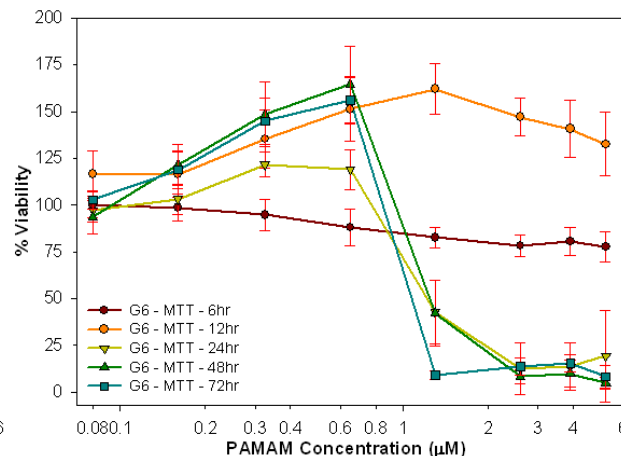
391 To analyse the effect this had on viability, AB and MTT assays were performed: Figure 8.

392

393 (a)



(b)



394 Figure 8: Alamar Blue (a) and MTT (b) dose dependent toxicity results for PAMAM G6  
395 dendrimers in HaCaT cells after 6, 12, 24, 48 and 72 hours. Viability is calculated as the

396 percentage of living cells as compared to a BSO control. The X-axis is plotted logarithmically to  
397 allow for better visualisation of lower doses. Data points are the mean of 18 samples, with error  
398 bars showing ( $\pm$ ) the standard deviation.  
399

400

401 The viability results of the PAMAM G6 dendrimers are similar to those observed in the G4  
402 analysis. In Figure 8, for 6 and 12 hour exposure, little toxicity is recorded by AB, although the  
403 response is significantly stronger at the later time points. The previously reported EC<sub>50</sub> obtained  
404 from the AB assay for PAMAM G6 dendrimers is in the range of 1µM-1.6µM at 24 hours,<sup>8</sup>  
405 which would appear to agree with the values obtained in this study. However, as was the case for  
406 PAMAM G4 exposure, the MTT assay registers increased percentage viability, compared to  
407 BSO control, for the intermediate doses, for all but the 6 hour exposure time point. A cytotoxic

408 response is elicited for doses greater than 1 $\mu$ M, for the 24, 48 and 72 hour time points and the  
409 response is consistent with the previously reported EC<sub>50</sub> values of 0.92 $\mu$ M-1.13 $\mu$ M.<sup>7</sup>

410

### 411 PAMAM G4-G6 Comparative Analysis

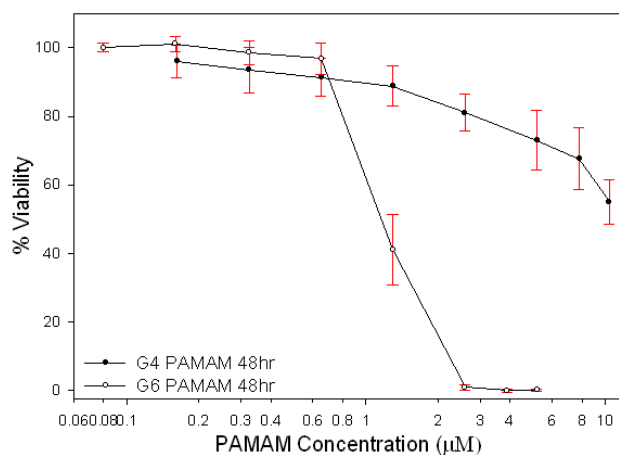
412 PAMAM nanoparticle toxicity is a generation dependant process,<sup>7,8,9</sup> therefore, a comparison of  
413 the response of BSO treated cells to G4 and G6 dendrimer exposure was performed, to establish  
414 whether a similar generation dependence of the cellular responses is still evident.

415

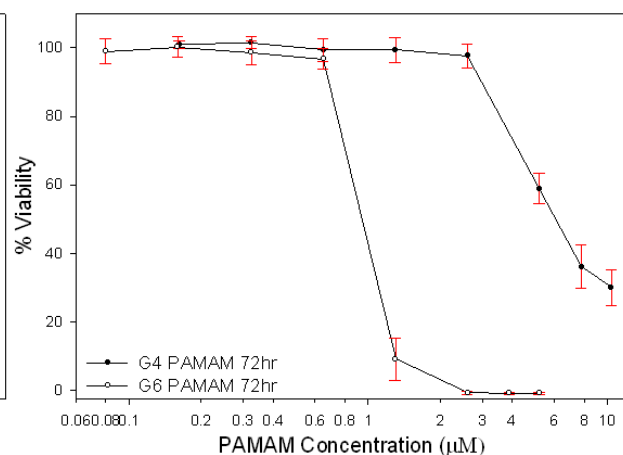
416 The AB and MTT assays were compared for PAMAM G4 and G6 dendrimers, and the results  
417 are shown in Figures 9 (AB) and 10 (MTT). For both dendrimers, approximately equivalent  
418 concentration ranges were used, although, for the PAMAM G6 dendrimers, a slightly lower  
419 initial concentration was used due to the higher associated toxicity.<sup>7,8,9,10</sup>

420

421 a)



b)



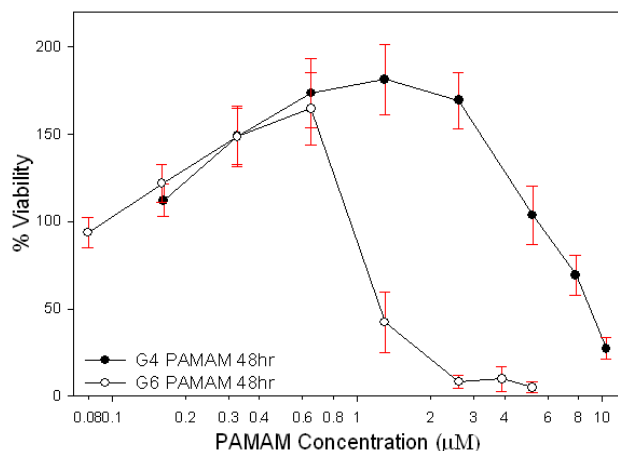
422

423 Figure 9: Alamar Blue (AB) dose dependant toxicity results comparing the PAMAM G4 and G6  
424 dendrimers in HaCaT cells after 48 hours (a) and 72 hours (b). Viability is calculated as the  
425 percentage of living cells as compared to BSO control. The x-axis is plotted logarithmically to

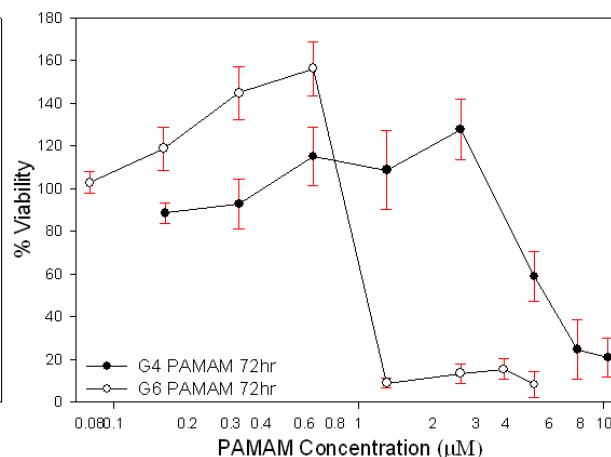
426 allow for better visualisation of lower doses. Data points are the mean of 18 samples, with error  
 427 bars showing ( $\pm$ ) the standard deviation. 6, 12 and 24 hour graphs can be seen in the  
 428 supplementary material section (Figure S6).  
 429  
 430 Little or no significant cytotoxicity was registered by the AB assay for either dendrimer at the 6  
 431 and 12 hour time points. At 24 hours, the higher toxicity associated with the G6 dendrimers  
 432 becomes apparent, while the G4 still shows no significant change (Supplementary Material:  
 433 Figure S6, c). At 48 hours (Figure 9(a)) the G4 dendrimers begin to elicit a significant toxic  
 434 response and finally, at 72 hours (Figure 9(b)), the G4 toxic profile is beginning to match that of  
 435 G6, although the reduction of viability is much higher for G6.

436

437 a)



b)



438 **Figure 10: MTT dose dependant toxicity results comparing the PAMAM G4 and G6 dendrimers**  
 439 **in HaCaT cells after 48 hours (a) and 72 hours (b). Viability is calculated as the percentage of**

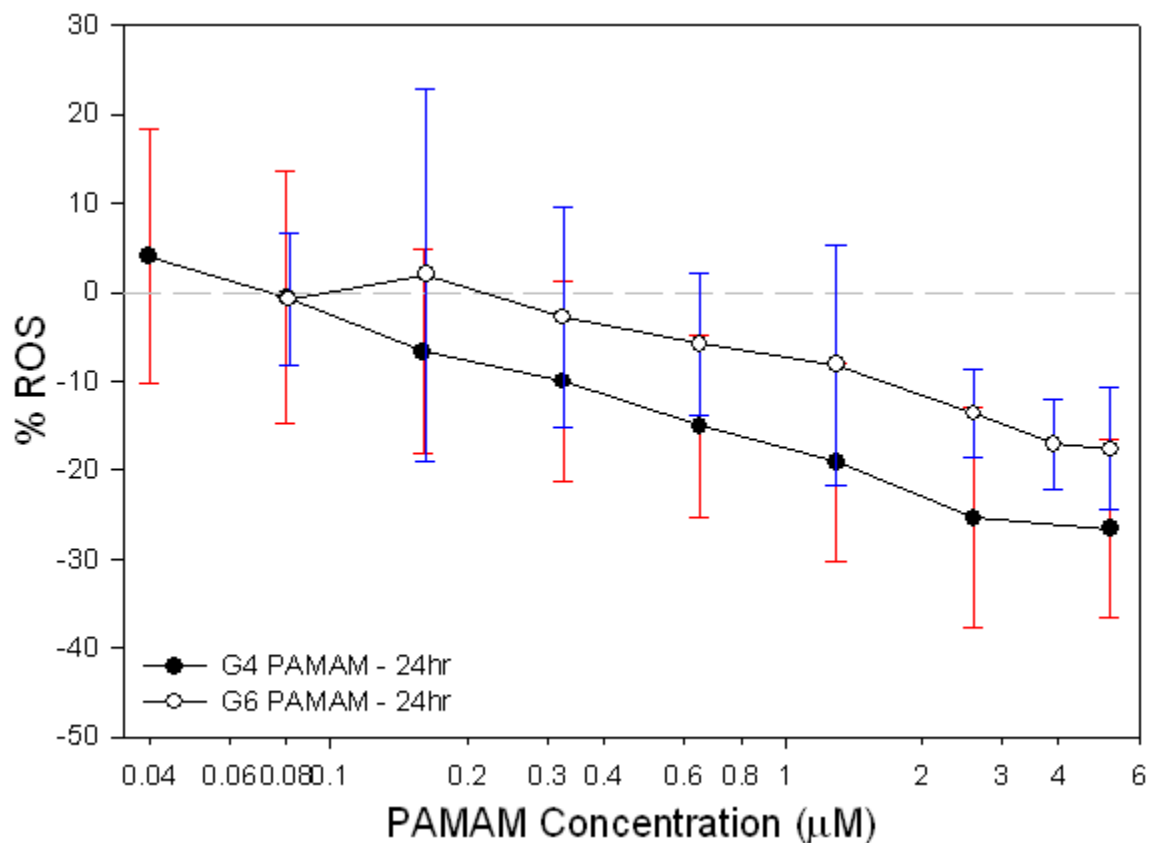
440 living cells as compared to BSO control. The X-axis is plotted logarithmically to allow for better  
 441 visualisation of lower doses. Data points are the mean of 18 samples, with error bars showing ( $\pm$ )  
 442 visualisation of lower doses. Data points are the mean of 18 samples, with error bars showing ( $\pm$ )

443 the standard deviation. 6, 12 and 24 hour graphs can be seen in the supplementary material  
444 section (Figure S7).

445

446 In the MTT, similar to AB response, no significant difference was seen in the 6 hour analysis for  
447 the two dendrimers, although differences become apparent at 12 hours (Supplementary Material:  
448 Figure S7, b), at which point the MTT response increases above that of controls for the G6  
449 dendrimer. This increase in MTT response also occurs for the G4 dendrimers, although, it is not  
450 manifest until the later time point of 48 hours (Figure 10(a)). Similar to the AB response,  
451 cytotoxicity is registered by the MTT assay for both dendrimers beginning at 24 hours; however,  
452 the AB only reaches about 50% viability. At 48 and 72 hours a more complete toxic profile for  
453 both assays is seen and distinct generation dependence is observable, more consistent with that  
454 observed for untreated cells.<sup>7</sup>

455



456  
 457 Figure 11: Dose dependant generation of ROS in HaCaT cells (shown at 24 hours for PAMAM  
 458 G4 and G6). Data is compared to BSO control which was set to equal 0%. The X-axis is plotted  
 459 logarithmically to allow for better visualisation of lower concentrations. Data points are the mean  
 460 of 18 samples, with error bars showing ( $\pm$ ) the standard deviation.

461  
 462 To further investigate any generation dependence, the dose response of the ROS was compared  
 463 for the G4 and the G6 (Figure 11). It is notable that the generation dependence of the trends is  
 464 reversed in Figure11 where G4 elicits a more pronounced reduction in ROS levels than G6.

465

## 466 Discussion

467 The confocal images of Figures: 1 and 2 (PAMAM G4) and Figures: 5 and 6 (PAMAM G6)  
468 show that, for cells treated with 200 $\mu$ M BSO for 18 hours prior to PAMAM exposure, the rate of  
469 endocytosis has been markedly reduced. This reduction in endocytosis is accompanied by a  
470 similar reduction in intracellular ROS and a dramatic change in the responses of the cytotoxic  
471 assays. Nevertheless, the observed reduction of intracellular ROS and cytotoxic responses are  
472 systematically dependent on dendrimer exposure time, dose and generation, consistent with the  
473 intracellular action of the dendritic nanoparticles.

474  
475 The demonstrated mechanism of PAMAM dendrimer toxicity is one of endocytosis,<sup>8,43,44</sup> ROS  
476 production,<sup>7,8,9,18</sup> subsequent endosomolysis, whereby the nanoparticle bursts out of the  
477 endosome/lysosome into the cytosol,<sup>19</sup> and localisation in the mitochondria.<sup>45</sup> Mukherjee and  
478 Byrne (2013) identified two apoptotic pathways, the death-receptor pathway (extrinsic, Fas  
479 mediated FADD pathway<sup>46</sup>) and the mitochondrial pathway (intrinsic, TNF- $\alpha$  mediated  
480 FADD<sup>47</sup>).<sup>10</sup> The former is initiated by the earlier stage ROS generation in the region of the  
481 endosomes, while the latter is initiated by the localisation of the dendrimers in the mitochondria.  
482 It has been proposed that the early stage ROS production is due to the action of NADPH  
483 oxidase<sup>6</sup> (producing superoxide anions (O<sub>2</sub><sup>-</sup>)<sup>48</sup>) and the v-ATPase proton pump (providing  
484 protons,<sup>49</sup> ultimately leading to production of H<sub>2</sub>O<sub>2</sub><sup>50</sup> in and around the endosome. In cells  
485 treated with BSO, however, PAMAM dendrimers elicit a dramatically different cytotoxicity  
486 profile, as registered by the AB and MTT assays, compared to that of untreated cells.<sup>7,8</sup>

487

488 Studies by Khalid *et al.* (2015) of cellular uptake of PPI dendrimers have demonstrated that,  
489 although the larger generation PPI dendrimers are endocytosed and elicit similar responses to  
490 PAMAM equivalents in HaCaT cells, for smaller generation PPI dendrimers, uptake by passive  
491 diffusion occurs and, when the dendrimers enter the cell in this way, they were observed to act as  
492 antioxidants and elicit a significantly reduced cytotoxic effect.<sup>18</sup> BSO exposure has been shown  
493 to permeabilise the cell membrane,<sup>28</sup> and as a result, it is proposed that the PAMAM G4 and G6  
494 dendrimers are able to circumvent the endocytotic process, are uptaken by passive diffusion, and,  
495 as PAMAM dendrimers are similar in structure to PPI dendrimers and have comparable surface  
496 chemistry, similarly behave as antioxidants in the cytosol, eliciting substantially reduced  
497 cytotoxic responses.

498

499 Alamar Blue is a non-specific assay and measures cellular viability based on the overall activity  
500 of the cytosolic environment.<sup>51</sup> The significant reduction, rather than expected increase, of  
501 toxicity as registered by this assay reflects the reduction in the endocytosis process (which  
502 initiates the Fas mediated FADD (death-receptor) apoptotic pathway), in favour of the passive  
503 diffusion of nanoparticles across the membrane, and consequent reduction in ROS generation in  
504 the region of endosomes. However, endocytosis is not fully eliminated for either generation, and  
505 therefore, the activation of the Fas mediated pathway, on a much reduced scale, would in part  
506 explain why the generation dependent response is still observed for the PAMAMs.

507

508 The MTT assay measures mitochondrial activity as an indicator of cellular viability<sup>52,53,54</sup> and, in  
509 the case of the studies described here, the mitochondria are implicated in at least two different  
510 processes and changes in MTT responses reflect the dose and generation dependence of these

511 processes at several time points. The first process is the loss of GSH from the cell, which has  
512 been shown to cause activation of mitochondrial signalling pathways and expression of genes  
513 associated with apoptosis, growth and differentiation.<sup>33,38,39,40</sup> This overall increase in  
514 mitochondrial activity (observed in the low dose regime), is seen as the initial increase in MTT  
515 values above controls, associated with dose and generation dependent decrease in ROS below  
516 controls, due to the antioxidant effect of the passively uptaken dendrimer nanoparticles.

517  
518 The second effect gives rise to a sharp decrease in mitochondrial activity (observed in the higher  
519 dose regime); consistent with PAMAM dendrimer localisation and disruption of the  
520 mitochondria,<sup>7,8</sup> initiating the mitochondrial apoptotic pathway, leading to cell death in a dose  
521 dependant fashion, as observed for untreated cells.<sup>7,8</sup> This process may be accelerated via the  
522 opening of the mitochondrial membrane permeability transition pore.<sup>30,31,32</sup> Whether passively  
523 diffused into the cell, or released into the cytosol by endosomolysis after endocytosis, the result  
524 of free PAMAM dendrimers in the cytosol and subsequent localisation to the mitochondria  
525 should be equivalent, both resulting in disruption of the mitochondria, a second phase increase in  
526 ROS within the cell, subsequent decay in the mitochondrial membrane potential and finally the  
527 initiation of a cascade leading to apoptosis.<sup>7,8,9,10</sup> It should also be noted that in both cases the  
528 opening of the mitochondrial membrane transition pore occurs, either by the action of  
529 BSO,<sup>30,31,32</sup> or due to the release of the endosomal/lysosomal contents causing intracellular  
530 release of Ca<sup>2+</sup>, leading to calcium dependant opening of the pore.<sup>21</sup> This would, in both cases,  
531 facilitate the entry of the dendrimer to the mitochondria. As a result, in the high dose regime, the  
532 observed toxic response of the BSO treated cells, as registered by the MTT assay, is not very  
533 different to that observed for untreated cells.



534

535 The passive diffusion of dendrimers across the cell membrane is a size dependant process<sup>18</sup> and,  
536 the generation dependence of the cellular responses to the two PAMAM dendrimer generations,  
537 G4 and G6, (Figures: 1, 2, 5 and 6), is consistent with a higher uptake rate for the G4 dendrimer  
538 than the G6. The greater reduction of intensity of Rab-5a-RFP compared to controls (with no  
539 BSO treatment), G4 dendrimers (70%) compared to G6 (60%), indicates a higher diffusion rate  
540 for G4 dendrimers, leaving fewer available for endocytosis. This further explains the higher rate  
541 of anti-oxidative activity exhibited by the G4 dendrimers when compared to G6 (Figure 11).  
542 Overall, it would appear that the membrane has become more permeable to an extent that favours  
543 passive uptake, although not completely eliminating active endocytosis.

544

545 Within the framework of Adverse Outcome Pathways (AOPs), recently endorsed by the  
546 OECD<sup>55,56</sup> as a method to simplify the representation of the mode of action of a toxicant or  
547 agonist, the generation of ROS can be considered the key Molecular Initiating Event (MIE) of  
548 the AOP, which ultimately leads to the AO of loss of cell viability. The treatment with BSO  
549 causes a depletion of GSH, which would lead to the expectation of much increased ROS levels  
550 after endocytosis. However, that was not observed and the result of the reduction of intrinsic  
551 GSH levels by BSO treatment was predominantly the increased permeability of the cell  
552 membrane, resulting in an increased rate of uptake of the PAMAM dendrimers by passive  
553 diffusion, making it a favoured uptake mechanism, more so for the smaller G4 dendrimer than  
554 the larger G6. The co-existence of the parallel uptake mechanisms increases the complexity of  
555 any model to describe the *in vitro* system, although it could prove a useful model to develop  
556 networks of AOPs, initiated by different MIEs. However, to fully examine the effect of reduction

557 of GSH in terms of decreased anti-oxidant activity alone, an assay which did not cause decrease  
558 of the permeabilisation of the cell membrane would be necessary.  
559  
560 Considering the potential for PAMAM dendrimers in nanomedical applications, it is important to  
561 note that, when diffused into the cell, the aminated surface chemistry of the dendrimers lend  
562 them antioxidant activity, similar to small molecular anti-oxidants, such as N-acetylcysteine  
563 (NAC) and NAC amide (NACA - a more bio-available version of NAC). NACA has been  
564 extensively studied as an antioxidant in the cell, due to its ability to diffuse across the membrane  
565 and the presence of a terminal proton donor group.<sup>57,58</sup> Interestingly, it has also been shown to  
566 completely reverse the damage caused to the cell by depletion of GSH.<sup>59,60,61</sup> NACA, due to this  
567 strong anti-oxidant ability, has been proposed in the treatment of several disorders and diseases,  
568 such as: HIV,<sup>62</sup> Alzheimer's and Parkinson's disease,<sup>60,63</sup> cataract formation,<sup>59</sup> retinal  
569 degeneration<sup>64</sup> and essentially any disease where ROS is identified as the potential MIE.<sup>(See: 61 and</sup>  
570 <sup>references therein)</sup> If PAMAM dendrimers are seen to act in a similar way, it may potentially allow for  
571 their use in a plethora of different nano-medical applications. As a strategy for drug release,  
572 endosomolysis can be extremely disruptive to the cell<sup>20</sup> and therefore, in the case of cationic  
573 nanoparticles for intracellular nanomedical applications, avoiding the process of endocytosis  
574 may be a valid strategy to pursue.<sup>22</sup> In terms of therapeutic applications, direct entry into the  
575 cytosol may be a more convenient route for drug or gene delivery.

576

577 Conclusions

578 Although PAMAM dendritic nanoparticles are known to elicit significant cytotoxic responses *in*  
579 *vitro*, the cellular response mechanisms can be notably altered by treatment of the cells with  
580 BSO. The treatment increases the cell membrane permeability, enabling uptake of the particles  
581 by passive diffusion, where after, they act as antioxidants in the cytosol, rather than producing  
582 oxidative stress in the region of endosomes. The ability to tune the cellular uptake mechanism  
583 allows direct entry into the cytosol and may have important implications for nanotoxicity as well  
584 as drug and gene delivery using nanovehicles.

585

586 Acknowledgements

587 The authors would like to thank Dr. Alan Casey and Esen Efeoglu for their contributions in the  
588 capturing and processing of the confocal images for this manuscript.

589

590 Funding Sources

591 Irish Government's Programme for Research in Third Level Institutions, Cycle 4, National  
592 Development Plan 2007-2013, supported by the European Union Structural Fund. M Maher is  
593 funded through the DIT Fiosraigh President's Award for Research Excellence 2010

594

595 Declaration of interest

596 The authors declare no conflict of interest related to the work presented in this manuscript.

597

## 598 References

- 599 1: Eichman, J.D., Bielinska, A.U., Kukowska-Latallo, J.F. and Baker, J.R.Jr. (2000) The use of  
600 PAMAM dendrimers in the efficient transfer of genetic material into cells. *J. Pharm. Sci.*  
601 *Technol.* 3(7): 233-245.
- 602
- 603 2: Duncan, R. and Izzo, L. (2005) Dendrimer biocompatibility and toxicity. *Adv. Drug. Deliv.*  
604 *Rev.* 57(15): 2215– 2237.
- 605
- 606 3: De Jong, W. H. and Borm, P.J.A. (2008) Drug delivery and nanoparticles: Applications and  
607 hazards. *Int. J. Nanomedicine.* 3(2): 133–149.
- 608
- 609 4: Nel, A., Xia, T., Mädler, L. and Li, N. (2006) Toxic potential of materials at the nanolevel.  
610 *Science.* 311(5761): 622-627.
- 611
- 612 5: Jain, K.K., Kesharwani, P., Gupta, U. and Jain, N.K. (2010) Dendrimer toxicity: Let's meet  
613 the challenge. *Int. J. Pharm.* 394(1-2): 122–142.
- 614
- 615 6: Xia, T., Kovichich, M., Brant, J., Hotze, M., Sempf, J., Oberley, T., Sioutas, C., Yeh, J.I.,  
616 Wiesner, M.R. and Nel, A.E. (2006) Comparison of the Abilities of Ambient and Manufactured  
617 Nanoparticles to Induce Cellular Toxicity According to an Oxidative Stress Paradigm. *Nano Lett.*  
618 6(8): 1794-1807.
- 619

620 7: Mukherjee, S.P., Davoren, M. and Byrne, H.J. (2010) *In vitro* mammalian cytotoxicological  
621 study of PAMAM dendrimers - towards quantitative structure activity relationships. *Toxicol. in*  
622 *Vitro*, 24(1): 169-177.

623

624 8: Mukherjee, S.P., Lyng, F.M., Garcia, A., Davoren, M. and Byrne H.J. (2010) Mechanistic  
625 studies of *in vitro* cytotoxicity of Poly(amidoamine) dendrimers in mammalian cells. *Toxicol.*  
626 *Appl. Pharmacol.* 248(3): 259–268.

627

628 9: Naha, P.C., Davoren, M., Lyng, F.M. and Byrne, H.J. (2010) Reactive Oxygen Species (ROS)  
629 induced cytokine production and cytotoxicity of PAMAM dendrimers in J774A.1 cells. *Toxicol.*  
630 *Appl. Pharmacol.* 246(1-2): 91-99

631

632 10: Mukherjee S.P. and Byrne, H.J. (2013) Polyamidoamine Dendrimer Nanoparticle  
633 Cytotoxicity, Oxidative Stress, Caspase Activation and Inflammatory Response: Experimental  
634 Observation and Numerical Simulation. *Nanomed. Nanotech. Biol. Med.* 9(2): 202-211.

635

636 11: Anguissola, S., Garry, D., Salvati, A., O'Brien, P.J. and Dawson, K.A. (2014) High Content  
637 Analysis Provides Mechanistic Insights on the Pathways of Toxicity Induced by Amine-  
638 Modified Polystyrene Nanoparticles. *PLoS ONE*, 9(9): e108025.  
639 doi:10.1371/journal.pone.0108025

640

641 12: Paget, V., Dekali, S., Kortulewski, T., Grall, R., Gamez, C., Blazy, K., Aguerre-Chariol, O.,  
642 Chevillard, S., Braun, A., Rat, P and Lacroix, G. (2015) Specific Uptake and Genotoxicity

643 Induced by Polystyrene Nanobeads with Distinct Surface Chemistry on Human Lung Epithelial  
644 Cells and Macrophages. *PLoS ONE*, 10(4): e0123297. doi:10.1371/journal.pone.0123297  
645  
646 13: Lunov, O., Syrovets, T., Loos, C., Beil, J., Delacher, M., Tron, K., Nienhaus, G.U.,  
647 Musyanovych, A., Mailänder, V., Landfester, K. and Simmet, T. (2011) Differential Uptake of  
648 Functionalized Polystyrene Nanoparticles by Human Macrophages and a Monocytic Cell Line.  
649 *ACS Nano*. 5(3): 1657-1669.  
650  
651 14: Nabeshi, H., Yoshikawa, T., Matsuyama, K., Nakazato, Y., Tochigi, S., Kondoh, S., Hirai,  
652 T., Akase, T., Nagano, K., Abe, Y., Yoshioka, Y., Kamada, H., Itoh, N., Tsunoda, S. and  
653 Tsutsumi, Y. (2011) Amorphous nanosilica induce endocytosis dependent ROS generation and  
654 DNA damage in human keratinocytes. *Part. Fibre Toxicol.* 8(1): 10 pages.  
655  
656 15: Mozdzan, M., Szemraj, J., Rysz, J., Stolarek, R.A. and Nowak, D. (2006) Anti-oxidant  
657 activity of spermine and spermidine re-evaluated with oxidising system involving iron and  
658 copper ions. *Int. J. Biochem. Cell Biol.* 38(1): 69-81.  
659  
660 16: Lotito, S.B. and Frei, B. (2004) Relevance of apple polyphenols as antioxidants in human  
661 plasma: contrasting in vitro and in vivo effects. *Free Radic. Biol. Med.* 36(2): 201-211.  
662  
663 17: Hipkiss AR. (2009) Carnosine and its possible roles in nutrition and health. *Adv. Food Nutr.*  
664 *Res.* 57(-): 87-154.  
665

666 18: Khalid, H., Mukherjee, S.P., O'Neill, L. and Byrne, H.J. (2015) Structural dependence of the  
667 *In vitro* cytotoxicity, oxidative stress and uptake mechanisms of Poly(propylene imine) dendritic  
668 nanoparticles. *J. Appl. Toxicol.* (in press - Accepted: October 2015)  
669

670 19: Watson, P., Jones, A.T. and Stephens, D.J. (2005) Intracellular trafficking pathways and drug  
671 delivery: fluorescence imaging of living and fixed cells. *Adv. Drug Deliver. Rev.* 57(1): 43-61.  
672

673 20: Mukherjee, S.P. (2012) Towards Structure Activity Relationships for *in vitro* Toxicity of  
674 Polyamidoamine Dendritic Nanoparticles. *Thesis (PhD)*, Dublin Institute of Technology: 2012.  
675 Dublin: DIT.  
676

677 21: Xia, T., Kovichich, M., Liong, M., Mädler, L., Gilbert, B., Shi, H., Yeh, J.I., Zink, J.I. and  
678 Nel, A.E. (2008) Comparison of the mechanism of toxicity of zinc oxide and cerium oxide  
679 nanoparticles based on dissolution and oxidative stress properties. *ACS Nano.* 2(10): 2121-2134.  
680

681 22: Guarnieri, D., Sabella, S., Muscetti, O., Belli, V., Malvindi, M.A., Fusco, S., De Luca, E.,  
682 Pompa, P.P. and Netti, P.A. (2014) Transport across the cell-membrane dictates nanoparticle fate  
683 and toxicity: a new paradigm in nanotoxicology. *Nanoscale.* 6(17): 10264-10273.  
684

685 23: Girard, P-M., Graindorge, D., Smirnova, V., Rigolet, P., Francesconi, S., Scanlon, S. and  
686 Sage, E. (2013) Oxidative Stress in Mammalian Cells Impinges on the Cysteines Redox State of  
687 Human XRCC3 Protein and on Its Cellular Localization. *PLoS ONE*, DOI:  
688 10.1371/journal.pone.0075751



689

690 24: He, Y-Y., Huang, J-L., Ramirez, D.C. and Chignell, C.F. (2003) Role of Reduced  
691 Glutathione Efflux in Apoptosis of Immortalized Human Keratinocytes Induced by UVA. *J.*  
692 *Biol. Chem.* 278(10): 8058–8064.

693

694 25: Madesh, M., Benard, O. and Balasubramanian, K.A. (1998) Glutathione modulates lipid  
695 composition of human colon derived HT-29 cells. *Int. J. Biochem. Cell Biol.* 30(12): 1345-1352.

696

697 26: Tobi, S.E., Paul, N. and McMillan T.J. (2000) Glutathione modulates the level of free  
698 radicals produced in UVA-irradiated cells. *J. Photochem. Photobiol. B.* 57(2-3): 102–112.

699

700 27: Li, X.Y., Donaldson, K., Rahman, I. and Mac Nee, W. (1994) An investigation of the role of  
701 glutathione in increased epithelial permeability induced by cigarette smoke *in vivo* and *in vitro*.  
702 *Am. J. Respir. Crit. Care Med.* 149(6): 1518-1525.

703

704 28: Zaman, G.J., Lankelma, J., van Tellingen, O., Beijnen, J., Dekker, H., Paulusma, C., Oude  
705 Elferink, R.P., Baas, F. and Borst, P. (1995) Role of glutathione in the export of compounds from  
706 cells by the multidrug-resistance-associated protein. *Proc. Natl. Acad. Sci. USA.* 92(17): 7690-  
707 7694.

708

709 29: Griffith, O.W. (1982) Mechanism of Action, Metabolism, and Toxicity of Buthionine  
710 Sulfoximine and Its Higher Homologs, Potent Inhibitors of Glutathione Synthesis. *J. Biol. Chem.*  
711 257(22): 13704-13712.

712

713 30: Armstrong, J.S. and Jones, D.P. (2002) Glutathione depletion enforces the mitochondrial  
714 permeability transition and causes cell death in Bcl-2 overexpressing HL60 cells. *FASEB J.*  
715 *16(10):* 1263-1265.

716

717 31: Chernyak, B.V. and Bernardi, P. (1996) The mitochondrial permeability transition pore is  
718 modulated by oxidative agents through both pyridine nucleotides and glutathione at two separate  
719 sites. *Eur. J. Biochem.* *238(3):* 623–630.

720

721 32: Reed, D.J. and Savage, M.K. (1995) Influence of metabolic inhibitors on mitochondrial  
722 permeability transition and glutathione status. *Biochim. Biophys. Acta.* *1271(1):* 43–50.

723

724 33: Circu, M.L. and Aw, T.Y. (2008) Glutathione and apoptosis. *Free Radic. Res.* *42(8):* 689–  
725 706.

726

727 34: Lash, L.H. (2006) Mitochondrial Glutathione Transport: Physiological, Pathological and  
728 Toxicological Implications. *Chem. Biol. Interact.* *163(1-2):* 54–67.

729

730 35: Beatrice, M.C., Stiers, D.L. and Pfeiffer, D.R. (1984) The role of glutathione in the retention  
731 of Ca<sup>2+</sup> by liver mitochondria. *J. Biol. Chem.* *259(2):* 1279–1287.

732

733 36: Lotscher, H.R., Winterhalter, K.H., Carafoli, E. and Richter, C. (1979) Hydroperoxides can  
734 modulate the redox state of pyridine nucleotides and the calcium balance in rat liver  
735 mitochondria. *Proc. Natl. Acad. Sci. USA*. 76(9): 4340–4344.  
736

737 37: Olafsdottir, K., Pascoe, G.A. and Reed, D.J. (1988) Mitochondrial glutathione status during  
738 Ca<sup>2+</sup> ionophore-induced injury to isolated hepatocytes. *Arch. Biochem. Biophys.* 263(1): 226–  
739 235.  
740

741 38: Davis, W.Jr., Ronai, Z. and Tew, K.D. (2001) Cellular thiols and reactive oxygen species in  
742 drug-induced apoptosis. *J. Pharmacol. Exp. Ther.* 296(1): 1–6.  
743

744 39: Petit, P.X., Susin, S.A., Zamzami, N., Mignotte, B. and Kroemer, G. (1996) Mitochondria  
745 and programmed cell death: Back to the future. *FEBS Lett.* 396(1): 7–13.  
746

747 40: Skulachev, V.P. (1996) Why are mitochondria involved in apoptosis? Permeability transition  
748 pores and apoptosis as selective mechanisms to eliminate superoxide-producing mitochondria  
749 and cells. *FEBS Lett.* 397(1): 7–10.  
750

751 41: Maher, M.A., Naha, P.C., Mukerjee, S.P. and Byrne, H.J. (2014) Numerical simulations of in  
752 vitro nanoparticle toxicity – the case of Poly(amido amine) dendrimers. *Toxicol. In Vitro.* 28(8):  
753 1449-1460.  
754

755 42: Zinchuk, V. and Zinchuk, O. (2008) Quantitative colocalization analysis of confocal  
756 fluorescence microscopy images. *Curr. Protoc. Cell Biol. Ch.4(Unit 4.19)*, 1-16.  
757

758 43: Kitchens, K.M., Foraker, A.B., Kolhatkar, R.B., Swaan, P.W., Ghandehari, H. (2007)  
759 Endocytosis and interaction of poly (Amidoamine) dendrimers with Caco-2 cells. *Pharmaceut.*  
760 *Res. 24(11)*: 2138–2145.  
761

762 44: Hong, S., Bielinska, A.U., Mecke, A., Keszler, B., Beals, J.L., Shi, X., Balogh, L., Orr, B.G.,  
763 Baker, J.R.Jr and Banaszak Holl, M.M. (2004) Interaction of poly(amidoamine) dendrimers with  
764 supported lipid bilayers and cells: hole formation and the relation to transport. *Bioconjugate*  
765 *Chem. 15(4)*: 774–782.  
766

767 45: Lee, J.H., Cha, K.E., Kim, M.S., Hong, H.W., Chung, D.J., Ryu, G. and Myung, H. (2009)  
768 Nanosized polyamidoamine (PAMAM) dendrimer-induced apoptosis mediated by mitochondrial  
769 dysfunction. *Toxicol. Lett. 190(2)*: 202–207.  
770

771 46: Wajant, H. (2002) The Fas signaling pathway: more than a paradigm. *Science*  
772 *296(5573)*:1635-1636.  
773

774 47: Desagher, S. and Martinou, J.C. (2000) Mitochondria as the central control point of  
775 apoptosis. *Trends Cell Biol. 10(9)*: 369-377.  
776

777 48: Shuvaev, V.V., Han, J., Yu, K.J., Huang, S., Hawkins, B.J., Madesh, M., Nakada, M. and  
778 Muzykantov, V.R. (2011) PECAM-targeted delivery of SOD inhibits endothelial inflammatory  
779 response. *FASEB J.* 25(1): 348-357.  
780

781 49: Nel, A.E., Mädler, L., Velegol, D., Xia, T., Hoek, E.M.V., Somasundaran, P., Klaessig, F.,  
782 Castranova, V. and Thompson, M. (2009) Understanding biophysicochemical interactions at the  
783 nano–bio interface. *Nature Materials.* 8(7): 543 – 557.  
784

785 50: Babior, B.M., Lambeth, J.D. and Nauseef, W. (2002) The neutrophil NADPH oxidase. *Arch.*  
786 *Biochem. Biophys.* 397(2): 342–344.  
787

788 51: O'Brien, J., Wilson, I., Orton, T. and Pognan, F. (2000) Investigation of the Alamar Blue  
789 (resazurin) fluorescent dye for the assessment of mammalian cell cytotoxicity. *Eur. J. Biochem.*  
790 267(17): 5421-5426.  
791

792 52: Mosmann, T. (1983) Rapid colorimetric assay for cellular growth and survival: Application  
793 to proliferation and cytotoxicity assays. *J. Immunol. Methods.* 65(1): 55-63.  
794

795 53: Denizot, F. and Lang, R. (1986) Rapid colorimetric assay for cell growth and survival:  
796 Modifications to the tetrazolium dye procedure giving improved sensitivity and reliability. *J.*  
797 *Immunol. Methods.* 89(2): 271-277.  
798

799 54: Hansen, M.B., Nielsen, S.E. and Berg, K. (1989) Re-examination and further development of  
800 a precise and rapid dye method for measuring cell growth/cell kill. *J. Immunol. Methods.* 119(2):  
801 203-210.

802

803 55: Organisation for Economic Co-Operation and Development (OECD): Guidance Document  
804 on the Validation of (Quantative) Structure Activity Relationships [(Q)SAR] Models, *OECD,*  
805 *ENV/JM/MONO(2007)2*, 2007.

806

807 56: Organisation for Economic Co-Operation and Development (OECD): Guidance Document  
808 On Developing and Assessing Adverse Outcome Pathways, *OECD, ENV/JM/MONO(2013)6*,  
809 2013.

810

811 57: Price, T.O., Uras, F., Banks, W.A. and Ercal, N. (2006) A novel antioxidant N-acetylcysteine  
812 amide prevents gp120- and Tat-induced oxidative stress in brain endothelial cells. *Exp. Neurol.*  
813 *201(1):* 193–202.

814

815 58: Grinberg, L., Fibach, E., Amer, J. and Atlas, D. (2005) N-acetylcysteine amide, a novel cell  
816 permeating thiol, restores cellular glutathione and protects human red blood cells from oxidative  
817 stress. *Free Radic. Biol. Med.* 38(1): 136–145.

818

819 59: Carey, J.W., Pinarci, E.Y., Penugonda, S., Karacal, H. and Ercal, N. (2011) *In vivo* inhibition  
820 of l-buthionine-(S,R)-sulfoximine-induced cataracts by a novel antioxidant, N-acetylcysteine  
821 amide. *Free Radic. Biol. Med.* 50(6): 722–729.

822

823 60: Penugonda, S., Mare, S., Goldstein, G., Banks, W.A. and Ercal, N. (2005) Effects of N-  
824 acetylcysteine amide (NACA), a novel thiol antioxidant against glutamate-induced cytotoxicity  
825 in neuronal cell line PC12. *Brain Research. 1056(2): 132–138.*

826

827 61: Sunitha, K., Hemshekhar, M., Thushara, R.M., Santhosh, M.S., Yariswamy, M., Kemparaju,  
828 K. and Girish, K.S. (2013) N-Acetylcysteine amide: a derivative to fulfill the promises of N-  
829 Acetylcysteine. *Free Radic. Res. 47(5): 357-367.*

830

831 62: Banerjee, A., Zhang, X., Manda, K.R., Banks, W.A. and Ercal, N. (2010) HIV proteins  
832 (gp120 and Tat) and methamphetamine in oxidative stress-induced damage in the brain: potential  
833 role of the thiol antioxidant N-acetylcysteine amide. *Free Radic. Biol. Med. 48(10): 1388-1398.*

834

835 63: Lee, K.S., Kim, S.R., Park, H.S., Park, S.J., Min, K.H., Lee, K.Y., Choe, Y.H., Hong, S.H.,  
836 Han, H.J., Lee, Y.R., Kim, J.S., Atlas, D. and Lee, Y.C. (2007) A novel thiol compound, N-  
837 acetylcysteine amide, attenuates allergic airway disease by regulating activation of NF-kappaB  
838 and hypoxia-inducible factor-1alpha. *Exp. Mol. Med. 39(6): 756-768.*

839

840 64: Schimel, A.M., Abraham, L., Cox, D., Sene, A., Kraus, C., Dace, D.S., Ercal, N. and Apte,  
841 R.S. (2011) N-acetylcysteine amide (NACA) prevents retinal degeneration by up-regulating  
842 reduced glutathione production and reversing lipid peroxidation. *Am. J. Pathol. 178(5): 2032-  
843 2043.*